

# A spectral-Galerkin turbulent channel flow solver for large-scale simulations

Mikael Mortensen<sup>a</sup>

<sup>a</sup>*Department of Mathematics, Division of Mechanics, University of Oslo*

---

## Abstract

A fully (pseudo-)spectral solver for direct numerical simulations of large-scale turbulent channel flows is described. The solver utilizes the Chebyshev base functions suggested by J. Shen [SIAM J. Sci. Comput., 16, 1, 1995], that lead to stable and robust numerical schemes, even at very large scale. New and fast algorithms for the direct solution of the linear systems are devised, and algorithms and matrices for all required scalar products and transforms are provided. We validate the solver for very high Reynolds numbers. Specifically, the solver is shown to reproduce the first order statistics of Hoyas and Jiménez [Phys. Fluids, 18(1), 2006], for a channel flow at  $Re_\tau = 2000$ . The solver is available through the open source project spectralDNS [<https://github.com/spectralDNS>].

*Keywords:* DNS, Fourier, Chebyshev, Biharmonic, Helmholtz, turbulence

---

## 1. Introduction

Direct Numerical Simulations (DNS) of turbulent flows is a very important research tool, utilized across a range of scientific communities [1]. DNS is used extensively to validate statistical models, and to further our understanding of complex mechanisms taking place inside turbulent flows. One of the many advantages of DNS is that it provides all information about a flow, and quantities that can be very hard to study experimentally, like velocity-pressure interactions, are trivially extracted from a DNS. In this regard, DNS both complements and extends the knowledge we are able to extract from experiments.

The most commonly known DNS use simple geometries, because turbulence physics may then most easily be isolated and studied. Isotropic and homogeneous turbulence are usually studied numerically in triply periodic domains, which allows for a spectral Fourier decomposition in all three spatial directions. Spectral methods are often favored in DNS due to their superior accuracy and resolution properties. One example is given in the DNS review of Moin and Mahesh [1], who report that, for similar accuracy in first derivatives, a second-order finite difference scheme requires approximately 5.5 times more points than Fourier, in each spatial direction, whereas for a 6<sup>th</sup> order Padé scheme the factor is about 1.6.

In this paper we will consider the pressure driven turbulent channel flow, where there are two periodic directions that can be handled with Fourier expansions, and a non-periodic wall-normal direction that requires a different type of discretization. There are many challenges associated with this inhomogeneity not faced by the pure Fourier solvers, but the first problem at hand is the discretization. Early DNS channel solvers, see, e.g., [2, 3, 4], typically used a Chebyshev expansion for the wall-normal direction and, as such, were still able to obtain spectral accuracy in all three

---

*Email address:* mikaem@math.uio.no (Mikael Mortensen)

spatial directions. A Chebyshev-tau technique, that utilize the recurrence relations of the Chebyshev polynomials, was used to approximate derivatives, and the coefficient matrices that appeared (tridiagonal) could then be inverted directly and efficiently [4]. A downside to the Chebyshev-tau method is usually quoted [5] as numerical instability and roundoff errors, caused by the recurrence relation, and severe condition numbers of the coefficient matrices. For Chebyshev-tau methods the condition numbers have been reported to grow with size as  $\mathcal{O}(N^8)$ , for a discretization using  $N$  points in the wall-normal direction. Discouraged by these numbers, all major recent channel flow simulations have found other, non-spectral, ways of discretizing the non-periodic direction.

The largest known channel simulations to date have been performed by Lee and Moser [6], where, for  $Re_\tau \approx 5200$ , they used a computational box of resolution  $[10240 \times 1530 \times 7680]$  for the streamwise, wall-normal and spanwise directions, respectively. Lee and Moser used seventh-order B-splines for the wall-normal direction. Other simulations of similar magnitude have been performed by Hoyas and Jiménez [7, 8], Lozano-Duran and Jiménez [9] and Bernardini, Pirozzoli and Orlandi [10]. Bernardini et al. used second-order finite differences throughout. The Jiménez group used dealiased Fourier in the two periodic directions and seventh-order compact finite differences, with fourth-order consistency and extended spectral-like resolution [11], for the wall-normal direction. The solver by Jiménez' group is reported to switch from Chebyshev to finite differences if the resolution is above a certain threshold [8] (reached around  $Re_\tau = 1000$ ). In other words, they attempt to use a fully spectral discretization for as large  $Re_\tau$  as possible. As previously mentioned, spectral methods are attractive for their accuracy and resolution properties, that are superior to those of any finite difference or spline method. As such, it is desirable to develop fully spectral solvers that can be used for large-scale turbulence simulations.

In his seminal papers [12, 13], Jie Shen describe how to construct Legendre and Chebyshev basis functions that lead to sparse matrices, susceptible to very fast direct solvers. To the author's knowledge, the bases have not been used for large-scale channel flow simulations, and algorithms for the required direct solvers have not, until now, been devised. Shen's bases have been used for the Navier Stokes equations before, though. Bouchon et.al. [14] describe a spectral-Galerkin formulation very similar to the one used in this paper. However, they choose the Legendre basis over Chebyshev, which has some consequences when aiming for large-scale, because fast transforms are required in moving from spectral to physical space, and back again. For Fourier and Chebyshev bases, the Fast Fourier Transforms (FFTs of  $\mathcal{O}(N \log N)$ ) apply directly. However, until recently, the discrete Legendre transforms required  $\mathcal{O}(N^2)$  operations. This scaling has now been improved by several authors, as recently reviewed by Hale and Townsend [15, 16], but the methods are still not quite on par with the FFTs. For example, Hale and Townsend describe an  $\mathcal{O}(N(\log N)^2 / \log \log N)$  algorithm, using intermediate fast transforms from Legendre to Chebyshev coefficients.

In this paper we will describe and assess a spectral-Galerkin channel flow solver based on Fourier and Shen's Chebyshev basis [13]. The solver will consist of parts that scale at worst as  $N \log N$ , for a 1D problem of size  $N$ , and as such as  $N^3 \log N$  for a 3D box of size  $N^3$ . We will give a proper description of the theoretical basis in Sec 2, the discretization of Navier-Stokes equations in Sec 3, and we will describe necessary algorithms, including a new fast direct solver for the biharmonic problem that arise, in Sec 4. We will finally show, in Sec 5, that roundoff is not a major issue, and that the Shen-Fourier spectral-Galerkin method is in deed applicable to large-scale simulations. The solver has been implemented in the open source code spectralDNS [17], where the bulk of the code is written in high-level Python [18], with critical parts migrated to Cython [19] for efficiency.

## 2. Basis functions and fast transforms

The Navier-Stokes equations, used to describe turbulent flow in a doubly periodic channel, can be written in rotational form as

$$\begin{aligned}\frac{\partial \mathbf{u}}{\partial t} &= \mathcal{H} + \nu \nabla^2 \mathbf{u} - \nabla \tilde{p}, \\ \nabla \cdot \mathbf{u} &= 0,\end{aligned}\tag{1}$$

where  $\mathbf{u}(\mathbf{x}, t) = (u, v, w)$  is the velocity vector,  $\mathbf{x} = (x, y, z)$  and  $t$  are position and time, and the nonlinearity  $\mathcal{H}(\mathbf{x}, t) = (\mathcal{H}_x, \mathcal{H}_y, \mathcal{H}_z) = \mathbf{u} \times \boldsymbol{\omega}$ , where  $\boldsymbol{\omega} = \nabla \times \mathbf{u}$ . The constant dynamic viscosity is denoted as  $\nu$  and  $\tilde{p}(\mathbf{x}, t)$  is a pressure modified to account for both the driving force,  $\beta(t)$ , and the kinetic energy, i.e.,  $\tilde{p} = p + \mathbf{u} \cdot \mathbf{u}/2 + \beta y$ , where  $p$  is the instantaneous pressure normalized by a constant density. The computational domain is  $\Omega = [-1, 1] \times [0, L_y] \times [0, L_z]$ , with channel walls located at  $x = \pm 1$ , such that no-slip applies at  $\mathbf{u}(\pm 1, y, z, t) = 0$ . The walls are spanning the  $y - z$  plane and the equations are periodic in the  $y$  and  $z$  directions with periodic lengths  $L_y$  and  $L_z$ , respectively.

The domain  $\Omega$  is discretized using  $N = (N_x, N_y, N_z)$  intervals, where the two periodic directions use uniform intervals. The computational mesh is given as

$$\begin{aligned}X_N &= \left\{ \mathbf{x} \in \mathbb{R}^3 | (x_i, y_j, z_k) = \left( h(i), \frac{jL_y}{N_y}, \frac{kL_z}{N_z} \right), \text{ where} \right. \\ &\quad \left. (i, j, k) \in [0, 1, \dots, N_x] \times [0, 1, \dots, N_y - 1] \times [0, 1, \dots, N_z - 1] \right\},\end{aligned}\tag{2}$$

where  $x_i = h(i)$  represents

$$h(i) = \begin{cases} \cos\left(\frac{i\pi}{N_x}\right) & \forall i = 0, 1, \dots, N_x \quad \text{for Chebyshev-Gauss-Lobatto points,} \\ \cos\left(\frac{(2i+1)\pi}{2N_x+2}\right) & \forall i = 0, 1, \dots, N_x \quad \text{for Chebyshev-Gauss points.} \end{cases}\tag{3}$$

The spectral-Galerkin method makes use of a three-dimensional scalar product in the weighted  $L^2_\sigma(\Omega)$  space, that is defined as

$$\langle u, v \rangle_\sigma = \int_\Omega u(\mathbf{x}) v^*(\mathbf{x}) \sigma(\mathbf{x}) dx dy dz,\tag{4}$$

where  $v^*$  is the complex conjugate of the test function  $v$  and the weights  $\sigma$  are unity for periodic directions and  $\sigma(x) = 1/\sqrt{1-x^2}$  for the inhomogeneous direction. In this work we will make use of the discrete weighted  $l^2_\sigma(\Omega)$  space, where quadrature is employed for the integration. As such, we redefine the scalar product as

$$\langle u, v \rangle_\sigma = \sum_{i=0}^{N_x} \sum_{j=0}^{N_y-1} \sum_{k=0}^{N_z-1} u(x_i, y_j, z_k) v^*(x_i, y_j, z_k) \sigma(x_i),\tag{5}$$

that is more amenable to the fast transforms that will be defined later in this section.

The Navier Stokes equations are discretized using Fourier basis functions for the periodic directions, and a combination of Chebyshev polynomials in the wall-normal direction. Three different sets of basis functions and function spaces are relevant for the wall-normal direction

$$\phi_k(x) = T_k(x), \quad W_{N_x} = \text{span}\{\phi_k\}_{k=0}^{N_x},\tag{6}$$

$$\bar{\phi}_k(x) = T_k(x) - T_{k+2}(x), \quad \bar{W}_{N_x} = \text{span}\{\bar{\phi}_k\}_{k=0}^{N_x-2},\tag{7}$$

$$\check{\phi}_k(x) = T_k(x) - \frac{2(k+2)}{k+3} T_{k+2}(x) + \frac{k+1}{k+3} T_{k+4}(x), \quad \check{W}_{N_x} = \text{span}\{\check{\phi}_k\}_{k=0}^{N_x-4},\tag{8}$$

where  $T_k(x)$  is the  $k$ 'th degree Chebyshev polynomial of the first kind. The basis functions and function spaces in (7) and (8) were suggested by Shen [13], and satisfy, respectively, the boundary conditions  $\bar{\phi}_k(\pm 1) = 0$ ,  $\check{\phi}_k(\pm 1) = 0$  and  $\check{\phi}'_k(\pm 1) = 0$ .

Three-dimensional basis functions and function spaces, that are periodic in  $y$  and  $z$  directions, can now be defined as

$$\psi_{\mathbf{k}}(\mathbf{x}) = \phi_l(x) e^{i(\underline{m}y + \underline{n}z)}, \quad V_N = \text{span}\{\psi_{\mathbf{k}}(\mathbf{x}) : \mathbf{k} \in K_N\}, \quad (9)$$

$$\bar{\psi}_{\mathbf{k}}(\mathbf{x}) = \bar{\phi}_l(x) e^{i(\underline{m}y + \underline{n}z)}, \quad \bar{V}_N = \text{span}\{\bar{\psi}_{\mathbf{k}}(\mathbf{x}) : \mathbf{k} \in \bar{K}_N\}, \quad (10)$$

$$\check{\psi}_{\mathbf{k}}(\mathbf{x}) = \check{\phi}_l(x) e^{i(\underline{m}y + \underline{n}z)}, \quad \check{V}_N = \text{span}\{\check{\psi}_{\mathbf{k}}(\mathbf{x}) : \mathbf{k} \in \check{K}_N\}, \quad (11)$$

where  $i = \sqrt{-1}$ . The wavenumbermesh,  $K_N$ , for space  $V_N$ , is defined by the Cartesian product of wavenumbers from the two periodic and the inhomogeneous wall-normal direction:  $K_N(l, m, n) = K^x(l) \times K^p(m, n)$ , where

$$K^p = \left\{ (\underline{m}, \underline{n}) = \left( \frac{2\pi m}{L_y}, \frac{2\pi n}{L_z} \right), \text{ where} \right. \\ \left. (m, n) \in \left[ -\frac{N_y}{2}, -\frac{N_y}{2} + 1, \dots, \frac{N_y}{2} - 1 \right] \times \left[ -\frac{N_z}{2}, -\frac{N_z}{2} + 1, \dots, \frac{N_z}{2} - 1 \right] \right\} \quad (12)$$

and  $K^x(l) = \{l \in \mathbb{Z} | l = 0, 1, \dots, N_x\}$ . The two remaining wavenumber meshes,  $\bar{K}_N$  and  $\check{K}_N$ , differ from  $K_N$  only in the range of the first index sets,  $\bar{K}^x$  and  $\check{K}^x$ , ending in  $N_x - 2$  and  $N_x - 4$ , respectively (see Eqs. (7) and (8)).

In the spectral-Galerkin method we look for solutions of the velocity components of the form

$$u(\mathbf{x}, t) = \frac{1}{N_y N_z} \sum_{\mathbf{k} \in \check{K}_N} \hat{u}_{\mathbf{k}}(t) \check{\psi}_{\mathbf{k}}(\mathbf{x}), \quad (13)$$

$$v(\mathbf{x}, t) = \frac{1}{N_y N_z} \sum_{\mathbf{k} \in \bar{K}_N} \hat{v}_{\mathbf{k}}(t) \bar{\psi}_{\mathbf{k}}(\mathbf{x}), \quad (14)$$

$$w(\mathbf{x}, t) = \frac{1}{N_y N_z} \sum_{\mathbf{k} \in \bar{K}_N} \hat{w}_{\mathbf{k}}(t) \bar{\psi}_{\mathbf{k}}(\mathbf{x}), \quad (15)$$

where  $\hat{u}_{\mathbf{k}}(t) = \hat{u}(l, m, n, t)$  are the expansion coefficients for the velocity component in  $x$ -direction (and similar for the other two components) and the scaling by  $N_y$  and  $N_z$  is merely for convenience and compliance with the definition used later for the inverse discrete Fourier transform. Note that from now on we will simply use the notation  $\hat{u}$  for  $\hat{u}_{\mathbf{k}}(t)$ , when it is possible to simplify without loss of clarity. Likewise we will simply use  $u$  for  $u(\mathbf{x}, t)$ .

For an efficient method it is crucial to be able to compute  $u$  quickly from  $\hat{u}$ , or, vice versa, to compute  $\hat{u}$  quickly from  $u$ . This may be achieved using the fast transform methods to be defined next. Consider first how to compute  $u$  from the known expansion coefficients  $\hat{u}$ . Writing out the summation terms, the expression (13) may be evaluated on the entire mesh (2) as

$$u(x_i, y_j, z_k, t) = \frac{1}{N_z} \sum_n \frac{1}{N_y} \sum_m \sum_l \underbrace{\hat{u}(l, m, n, t) \check{\phi}_l(x_i) e^{i\underline{m}y_j} e^{i\underline{n}z_k}}_{\check{\mathcal{S}}_x^{-1}} \quad \forall \mathbf{x} \in X_N, \\ \underbrace{\hspace{10em}}_{\mathcal{F}_y^{-1}} \\ \underbrace{\hspace{10em}}_{\mathcal{F}_z^{-1}} \\ u = \check{\mathcal{T}}^{-1}(\hat{u}) = \mathcal{F}_z^{-1}(\mathcal{F}_y^{-1}(\check{\mathcal{S}}_x^{-1}(\hat{u}))), \quad (16)$$

where  $\check{\mathcal{T}}^{-1}$  is used as short notation for the complete inverse transform in space  $\check{V}_N$ , and  $\mathcal{F}_y^{-1}$  and  $\mathcal{F}_z^{-1}$  represent inverse discrete Fourier transforms along directions  $y$  and  $z$  respectively. For simplicity, we have introduced here a special notation called the inverse *Shen* transform,  $\mathcal{S}_x^{-1}$ , that is used to transform coefficients from spectral to physical space in a series expansion that is using either one of the bases in (6, 7, 8). The inverse Shen transform,  $\mathcal{S}_x^{-1}$ , is performed along the wall-normal  $x$  direction, and it may be computed using fast Chebyshev transforms for all the three bases in (6, 7, 8), see Alg 6 in the Appendix. The transforms are slightly different for the three bases and  $\mathcal{S}_x^{-1}$ ,  $\check{\mathcal{S}}_x^{-1}$  and  $\check{\mathcal{S}}_x^{-1}$  are used to distinguish between them with obvious notation. Similarly,  $\check{\mathcal{T}}^{-1}$  and  $\mathcal{T}^{-1}$  define the inverse transforms for spaces  $\check{V}_N$  and  $V_N$ . Note that a transform in any one direction is performed over all indices in the other two directions. For example, for the transform in the  $x$ -direction we have

$$u(x_i, m, n, t) = \check{\mathcal{S}}_x^{-1}(\hat{u}(l, m, n, t)) \quad \forall i \in [0, 1, \dots, N_x] \text{ and } m, n \in K^p, \quad (17)$$

and similar for the other two directions.

Fast transforms may also be used in the scalar product defined in Eq. (5), using basis  $\check{\psi}_{\mathbf{k}}$  for  $v$

$$\begin{aligned} \left\langle u, \check{\psi}_{\mathbf{k}} \right\rangle_{\sigma} &= h \underbrace{\sum_i \sum_j \underbrace{\sum_k}_{\mathcal{F}_n} u(x_i, y_j, z_k, t) e^{-i n z_k} e^{-i m y_j}}_{\mathcal{F}_m} \check{\phi}_l(x_i) \sigma(x_i) \quad \forall \mathbf{k} \in \check{K}_N, \\ &= h \check{\mathcal{S}}(u) = h \check{\mathcal{S}}_l(\mathcal{F}_m(\mathcal{F}_n(u))). \end{aligned} \quad (18)$$

Here  $h \check{\mathcal{S}}(\cdot)$  denotes the complete three-dimensional scalar product and  $h = L_y L_z N_y^{-1} N_z^{-1}$  is a constant.  $\mathcal{F}_n$  and  $\mathcal{F}_m$  represent discrete Fourier transforms in  $z$ - and  $y$ -directions, respectively, and  $\check{\mathcal{S}}_l(\cdot) = (\cdot, \check{\phi}_l)_{\sigma}$  is used to represent the forward *Shen* scalar product in the  $x$ -direction. The weights,  $\sigma(x_i)$ , required for the Shen transforms, are defined as

$$\sigma(x_i) = \begin{cases} \frac{\pi}{c_i N_x} & \forall i = 0, 1, \dots, N_x \text{ for Chebyshev-Gauss-Lobatto points,} \\ \frac{\pi}{N_x + 1} & \forall i = 0, 1, \dots, N_x \text{ for Chebyshev-Gauss points,} \end{cases} \quad (19)$$

where  $c_0 = c_{N_x} = 2$  and  $c_i = 1$  for  $0 < i < N_x$ , see Sec. 1.11 of [20].

The scalar product  $h \check{\mathcal{S}}$  in (18) does not represent a complete transform. To find a transformation from physical  $u$  to spectral  $\hat{u}$ , we make use of Eq. (13) directly on the left hand side of (18) and use extensively the discrete orthogonality of the Fourier basis functions

$$\begin{aligned} \left\langle u, \check{\psi}_{\mathbf{k}} \right\rangle_{\sigma} &= \frac{1}{N_y N_z} \left\langle \sum_{(q,r,s) \in \check{K}_N} \hat{u}(q, r, s, t) \check{\psi}(q, r, s), \check{\psi}(l, m, n) \right\rangle_{\sigma} \quad \forall \mathbf{k} \in \check{K}_N, \\ &= h \sum_{q=0}^{N_x-4} \sum_{i=0}^{N_x} \check{\phi}_q(x_i) \check{\phi}_l(x_i) \sigma(x_i) \hat{u}(q, m, n, t), \\ &= h \sum_{q=0}^{N_x-4} \check{B}_{lq} \hat{u}(q, m, n, t). \end{aligned} \quad (20)$$

Here  $\check{B}_{lq} = (\check{\phi}_q, \check{\phi}_l)_{\sigma} = \sum_{i=0}^{N_x} \check{\phi}_q(x_i) \check{\phi}_l(x_i) \sigma(x_i)$  are the components of a banded mass matrix with only 5 nonzero diagonals, see Table 6. The complete transformation is now obtained by setting Eq.

(20) equal to (18) and solving for  $\hat{u}$ . Moving to matrix notation we get

$$h \sum_{q=0}^{N_x-4} \check{B}_{lq} \hat{u}(q, m, n, t) = h \check{S}(u)(l, m, n, t) \quad \forall \mathbf{k} \in \check{K}_N,$$

$$\hat{u} = \check{T}(u) = \check{B}^{-1} \check{S}(u), \quad (21)$$

where  $\check{T}(u)$  denotes the complete transformation, such that  $u = \check{T}^{-1}(\check{T}(u))$ . Note that, since  $\check{B}$  assembles to a pentadiagonal matrix for its decoupled odd and even coefficients, the solution ( $\check{B}^{-1}$ ) can be obtained very fast and the complete transformation thus requires a fast Chebyshev transform ( $\mathcal{O}(N_x \log N_x)$ ) and a fast linear algebraic solve ( $\mathcal{O}(N_x)$ ) for the wall-normal direction, given  $m$  and  $n$ . Similar transforms  $\mathcal{T}$  and  $\bar{\mathcal{T}}$  are defined for the two other bases (6) and (7), using mass matrices with components  $B_{lq} = (T_q, T_l)_\sigma$  (diagonal) and  $\bar{B}_{lq} = (\bar{\phi}_l, \bar{\phi}_q)_\sigma$  (three non-zero diagonals) and scalar products  $\mathcal{S}_l(\cdot) = (\cdot, T_l)_\sigma$  and  $\bar{\mathcal{S}}_l(\cdot) = (\cdot, \bar{\phi}_l)_\sigma$ . See Alg. 5 and 6 in the Appendix for algorithms for all required transforms.

### 3. Discretization of Navier Stokes equations

The Navier Stokes equations (1) are solved using a scheme proposed by Kim, Moin and Moser [4]. This scheme is developed by taking the Laplacian of the wall-normal momentum equation and the curl of the momentum equation. Following elimination of the pressure, the equations to solve are

$$\frac{\partial}{\partial t} \nabla^2 u = h_u + \nu \nabla^4 u, \quad (22)$$

$$\frac{\partial g}{\partial t} = h_g + \nu \nabla^2 g, \quad (23)$$

$$f + \frac{\partial u}{\partial x} = 0, \quad (24)$$

where

$$f = \frac{\partial v}{\partial y} + \frac{\partial w}{\partial z}, \quad (25)$$

$$g = \frac{\partial w}{\partial y} - \frac{\partial v}{\partial z}, \quad (26)$$

$$h_u = -\frac{\partial}{\partial x} \left( \frac{\partial \mathcal{H}_y}{\partial y} + \frac{\partial \mathcal{H}_z}{\partial z} \right) + \left( \frac{\partial^2}{\partial y^2} + \frac{\partial^2}{\partial z^2} \right) \mathcal{H}_x, \quad (27)$$

$$h_g = \frac{\partial \mathcal{H}_z}{\partial y} - \frac{\partial \mathcal{H}_y}{\partial z}. \quad (28)$$

The two remaining velocity components are computed from the definitions of  $f$  and  $g$ . The biharmonic equation (22) is solved with boundary conditions  $u(\pm 1) = u'(\pm 1) = 0$ , where the Neumann conditions follow from the continuity equation. The boundary conditions for Eq. (23) are  $g(\pm 1) = 0$ .

We consider the spectral-Galerkin discretization of (22), (23) and (24), using a central difference in time, with Crank-Nicolson for the linear terms and an Adams-Bashforth method for the nonlinear terms. To this end, the discretization in time is performed with a constant time step  $\Delta t > 0$ , such that time is represented discretely as  $t_\kappa = \kappa \Delta t$ ,  $\kappa \in [0, 1, \dots]$ , and variables with a time superscript, like  $u^\kappa = u(t_\kappa)$ . We get the variational formulation: with  $u^0(\mathbf{x})$ ,  $u^1(\mathbf{x})$ ,  $g^0(\mathbf{x})$  and  $g^1(\mathbf{x})$  given, for all

$\kappa > 1$  find  $u^{\kappa+1} \in \check{V}_N$ ,  $g^{\kappa+1} \in \bar{V}_N$  and  $f^{\kappa+1} \in \bar{V}_N$  such that

$$\left\langle \frac{\nabla^2(u^{\kappa+1} - u^\kappa)}{\Delta t}, \check{\psi}_{\mathbf{k}} \right\rangle_\sigma = \left\langle h_u^{\kappa+\frac{1}{2}}, \check{\psi}_{\mathbf{k}} \right\rangle_\sigma + \nu \left\langle \nabla^4 u^{\kappa+\frac{1}{2}}, \check{\psi}_{\mathbf{k}} \right\rangle_\sigma \quad \forall \psi_{\mathbf{k}} \in \check{V}_N, \quad (29)$$

$$\left\langle \frac{g^{\kappa+1} - g^\kappa}{\Delta t}, \bar{\psi}_{\mathbf{k}} \right\rangle_\sigma = \left\langle h_g^{\kappa+\frac{1}{2}}, \bar{\psi}_{\mathbf{k}} \right\rangle_\sigma + \nu \left\langle \nabla^2 g^{\kappa+\frac{1}{2}}, \bar{\psi}_{\mathbf{k}} \right\rangle_\sigma \quad \forall \psi_{\mathbf{k}} \in \bar{V}_N, \quad (30)$$

$$\left\langle f^{\kappa+1}, \bar{\psi}_{\mathbf{k}} \right\rangle_\sigma = \left\langle \frac{\partial u^{\kappa+1}}{\partial x}, \bar{\psi}_{\mathbf{k}} \right\rangle_\sigma \quad \forall \psi_{\mathbf{k}} \in \bar{V}_N. \quad (31)$$

Here superscript  $\kappa + \frac{1}{2}$  is used to represent Crank-Nicolson for linear terms (e.g.,  $u^{\kappa+\frac{1}{2}} = 0.5(u^{\kappa+1} + u^\kappa)$ ) and Adams-Bashforth for nonlinear (e.g.,  $h_u^{\kappa+\frac{1}{2}} = 1.5h_u^\kappa - 0.5h_u^{\kappa-1}$ ).

With  $f^{\kappa+1}$  and  $g^{\kappa+1}$  known, the two remaining velocity components are then computed by projection to the Dirichlet space  $\bar{V}_N$ : Find  $v^{\kappa+1} \in \bar{V}_N$  and  $w^{\kappa+1} \in \bar{V}_N$  such that

$$\left\langle f^{\kappa+1}, \bar{\psi}_{\mathbf{k}} \right\rangle_\sigma = \left\langle \frac{\partial v^{\kappa+1}}{\partial y} + \frac{\partial w^{\kappa+1}}{\partial z}, \bar{\psi}_{\mathbf{k}} \right\rangle_\sigma \quad \forall \bar{\psi}_{\mathbf{k}} \in \bar{V}_N, \quad (32)$$

$$\left\langle g^{\kappa+1}, \bar{\psi}_{\mathbf{k}} \right\rangle_\sigma = \left\langle \frac{\partial w^{\kappa+1}}{\partial y} - \frac{\partial v^{\kappa+1}}{\partial z}, \bar{\psi}_{\mathbf{k}} \right\rangle_\sigma \quad \forall \bar{\psi}_{\mathbf{k}} \in \bar{V}_N, \quad (33)$$

which simplifies considerably because all the derivatives are in periodic directions. Written in spectral space Eqs. (32) and (33) become simply the algebraic expressions

$$\hat{f}_{\mathbf{k}}^{\kappa+1} = \underline{m} \hat{v}_{\mathbf{k}}^{\kappa+1} + \underline{n} \hat{w}_{\mathbf{k}}^{\kappa+1} \quad \forall \mathbf{k} \in \bar{K}_N^0, \quad (34)$$

$$\hat{g}_{\mathbf{k}}^{\kappa+1} = \underline{m} \hat{w}_{\mathbf{k}}^{\kappa+1} - \underline{n} \hat{v}_{\mathbf{k}}^{\kappa+1} \quad \forall \mathbf{k} \in \bar{K}_N^0, \quad (35)$$

where  $\bar{K}_N^0$  is used to denote that these equations can be solved for all wavenumbers except  $m = n = 0$ . For  $m = n = 0$  we solve instead the momentum equations in  $y$  and  $z$  directions (see Eq. (1)):

$$\left\langle \frac{v^{\kappa+1} - v^\kappa}{\Delta t}, \psi_{\mathbf{k}} \right\rangle_\sigma = \left\langle \mathcal{H}_y^{\kappa+\frac{1}{2}}, \psi_{\mathbf{k}} \right\rangle_\sigma + \nu \left\langle \nabla^2 v^{\kappa+\frac{1}{2}}, \psi_{\mathbf{k}} \right\rangle_\sigma - \left\langle \beta^{\kappa+1}, \psi_{\mathbf{k}} \right\rangle_\sigma \quad \forall \mathbf{k} \in \bar{K}^x \times K^p(0,0), \quad (36)$$

$$\left\langle \frac{w^{\kappa+1} - w^\kappa}{\Delta t}, \psi_{\mathbf{k}} \right\rangle_\sigma = \left\langle \mathcal{H}_z^{\kappa+\frac{1}{2}}, \psi_{\mathbf{k}} \right\rangle_\sigma + \nu \left\langle \nabla^2 w^{\kappa+\frac{1}{2}}, \psi_{\mathbf{k}} \right\rangle_\sigma \quad \forall \mathbf{k} \in \bar{K}^x \times K^p(0,0). \quad (37)$$

Note that the regular pressure is eliminated since  $m = n = 0$ , and that (36) is the only place where the driving force, or the mean pressure gradient,  $\beta$ , enters the equations. Also, since  $\beta$  is constant in space, the term  $\langle \beta^{\kappa+1}, \bar{\psi}_{\mathbf{k}} \rangle_\sigma$  will only be non-zero for  $l = m = n = 0$ .

The final step of the method is to rewrite all equations on matrix form, using one-dimensional scalar products. Inserting the expansion (13) for  $u$  in  $\check{V}_N$ , and similar for  $g, h_u$  and  $h_g$  in  $\bar{V}_N$ , the inner products required to solve Eqs. (29-31) are

$$\left\langle \nabla^4 u, \check{\psi}_{\mathbf{k}} \right\rangle_\sigma = h \left[ \left( \check{\phi}_q''''', \check{\phi}_l \right)_\sigma - 2(\underline{m}^2 + \underline{n}^2) \left( \check{\phi}_q'', \check{\phi}_l \right)_\sigma + (\underline{m}^2 + \underline{n}^2)^2 \left( \check{\phi}_q, \check{\phi}_l \right)_\sigma \right] \hat{u}_q, \quad (38)$$

$$\left\langle \nabla^2 u, \check{\psi}_{\mathbf{k}} \right\rangle_\sigma = h \left[ \left( \check{\phi}_q'', \check{\phi}_l \right)_\sigma - (\underline{m}^2 + \underline{n}^2) \left( \check{\phi}_q, \check{\phi}_l \right)_\sigma \right] \hat{u}_q, \quad (39)$$

$$\left\langle \nabla^2 g, \bar{\psi}_{\mathbf{k}} \right\rangle_\sigma = h \left[ \left( \bar{\phi}_q'', \bar{\phi}_l \right)_\sigma - (\underline{m}^2 + \underline{n}^2) \left( \bar{\phi}_q, \bar{\phi}_l \right)_\sigma \right] \hat{g}_q, \quad (40)$$

$$\left\langle \frac{\partial u}{\partial x}, \bar{\psi}_{\mathbf{k}} \right\rangle_\sigma = h \left( \check{\phi}_q', \bar{\phi}_l \right)_\sigma \hat{u}_q, \quad (41)$$

$$\left\langle h_u, \check{\psi}_{\mathbf{k}} \right\rangle_\sigma = h \left[ -(\underline{m}^2 + \underline{n}^2) \left( \bar{\phi}_q, \check{\phi}_l \right)_\sigma \hat{\mathcal{H}}_{x,q} - \underline{m} \left( \bar{\phi}_q', \check{\phi}_l \right)_\sigma \hat{\mathcal{H}}_{y,q} - \underline{n} \left( \bar{\phi}_q', \check{\phi}_l \right)_\sigma \hat{\mathcal{H}}_{z,q} \right], \quad (42)$$

$$\left\langle h_g, \bar{\psi}_{\mathbf{k}} \right\rangle_\sigma = h \left[ \underline{m} \left( \bar{\phi}_q, \bar{\phi}_l \right)_\sigma \hat{\mathcal{H}}_{z,q} - \underline{n} \left( \bar{\phi}_q, \bar{\phi}_l \right)_\sigma \hat{\mathcal{H}}_{y,q} \right], \quad (43)$$

where for brevity in notation (as before) it is understood that the scalar products act along the first dimension of the transformed variables, i.e.,  $(\check{\phi}'_q, \bar{\phi}_l)_\sigma \hat{u}_q$  is short for the matrix vector product  $\sum_{q=0}^{N_x-4} (\check{\phi}'_q, \bar{\phi}_l)_\sigma \hat{u}(q, m, n, t)$ , for all  $m$  and  $n$ . The scalar products are used to set up linear systems of equations for the inhomogeneous wall-normal direction. All scalar products  $(\cdot, \cdot)_\sigma$  can be represented by sparse matrices. The required matrices with components  $\check{B}_{lq} = (\check{\phi}_q, \check{\phi}_l)_\sigma$ ,  $\bar{B}_{lq} = (\bar{\phi}_q, \bar{\phi}_l)_\sigma$ ,  $\check{M}_{lq} = (\check{\phi}_q, \check{\phi}_l)_\sigma$ ,  $\bar{C}_{lq} = (\check{\phi}'_q, \bar{\phi}_l)_\sigma$  and  $\check{C}_{lq} = (\check{\phi}'_q, \check{\phi}_l)_\sigma$  are given in Table 6,  $\check{A}_{lq} = -(\check{\phi}''_q, \check{\phi}_l)_\sigma$ ,  $\bar{A}_{lq} = -(\bar{\phi}''_q, \bar{\phi}_l)_\sigma$  are given in [13], whereas  $\check{Q}_{lq} = (\check{\phi}''''_q, \check{\phi}_l)_\sigma$  is given below in Eqs (57)-(60). Note that the matrices are computed using quadrature, which has some implications for Chebyshev-Gauss-Lobatto (GL) points, where the rows of the highest modes differ from those presented in Lemma 2.1 and 3.1 of [13]. This disagreement, that follows from inexact quadrature at the highest mode, explains the inclusion of the  $c_{k+4}$  term for matrix  $\check{B}$  and the  $c_{k+2}$  term for matrix  $\bar{B}$ . The matrix with components  $B_{lq} = (T_q, T_l)_\sigma$  is also different in the highest mode from Eq. 2.7 of [13], but agrees with Eqs. 1.135 and 1.136 of [20].

Assembling all scalar products, the final matrix form of Eqs. (29), (30) and (31), that can be used to solve for  $\hat{u}^{\kappa+1}$ ,  $\hat{g}^{\kappa+1}$  and  $\hat{f}^{\kappa+1}$ , given wavenumbers  $m$  and  $n$ , are now found as

$$\check{H}\hat{u}^{\kappa+1} = \left(2\check{A} - 2\check{z}^2\check{B} - \check{H}\right)\hat{u}^\kappa + \Delta t\check{S}(h_v^{\kappa+1/2}) \quad \forall \mathbf{k} \in \check{K}_N, \quad (44)$$

$$\bar{H}\hat{g}^{\kappa+1} = (2\bar{B} - \bar{H})\hat{g}^\kappa + \Delta t\bar{S}(h_g^{\kappa+1/2}) \quad \forall \mathbf{k} \in \bar{K}_N, \quad (45)$$

$$\bar{B}\hat{f}^{\kappa+1} = \bar{C}\hat{u} \quad \forall \mathbf{k} \in \bar{K}_N. \quad (46)$$

The coefficient matrices are given as

$$\check{H}(m, n) = -\frac{\nu\Delta t}{2}\check{Q} + (1 + \nu\Delta t\check{z}^2)\check{A} - \frac{2\check{z}^2 + \nu\Delta t\check{z}^4}{2}\check{B} \quad \forall m, n \in K^p, \quad (47)$$

$$\bar{H}(m, n) = -\frac{\nu\Delta t}{2}\bar{A} + (1 + \frac{\nu\Delta t\bar{z}^2}{2})\bar{B} \quad \forall m, n \in K^p, \quad (48)$$

where  $\check{z}^2 = \underline{m}^2 + \underline{n}^2$ . Equations (36) and (37) are also written on matrix form as

$$\bar{H}\hat{v}^{\kappa+1} = (2\bar{B} - \bar{H})\hat{v}^\kappa + \Delta t\bar{B}\hat{\mathcal{H}}_y^{\kappa+\frac{1}{2}} - \Delta t\bar{S}(\beta^{\kappa+1}) \quad \forall l \in \bar{K}^x, m = n = 0, \quad (49)$$

$$\bar{H}\hat{w}^{\kappa+1} = (2\bar{B} - \bar{H})\hat{w}^\kappa + \Delta t\bar{B}\hat{\mathcal{H}}_z^{\kappa+\frac{1}{2}} \quad \forall l \in \bar{K}^x, m = n = 0. \quad (50)$$

Finally, the nonlinear terms are computed with the recipes given in Eqs. (42, 43). To this end the required vector  $\hat{\mathcal{H}}$  is found by projecting to the Dirichlet vector space  $\check{V}_N^3$ , which corresponds to transforming the nonlinear cross product, evaluated in real space, over the entire mesh

$$\hat{\mathcal{H}}_i = \check{T}((\mathbf{u} \times \boldsymbol{\omega})_i) \quad \forall i = x, y, z. \quad (51)$$

The curl,  $\boldsymbol{\omega} = (g, \partial_z u - \partial_x w, \partial_y u - \partial_x v)$ , is computed by projecting each individual term to its appropriate spectral space, before transforming back to physical space. To this end, the two terms  $\partial_x v$  and  $\partial_x w$  are projected to  $V_N$  (requires  $C_{lq} = (\check{\phi}'_j, T_k)_\sigma$ , see Tab. 6), whereas the remaining  $\partial_y u$  and  $\partial_z u$  are projected to  $\check{V}_N$ . With compact notation using the transforms, we obtain

$$\partial_x v(\mathbf{x}) = \mathcal{T}^{-1}(B^{-1}C\hat{v}) \quad \forall \mathbf{x} \in X_N, \quad (52)$$

$$\partial_x w(\mathbf{x}) = \mathcal{T}^{-1}(B^{-1}C\hat{w}) \quad \forall \mathbf{x} \in X_N, \quad (53)$$

$$\partial_y u(\mathbf{x}) = \check{T}^{-1}(i\underline{m}\hat{u}) \quad \forall \mathbf{x} \in X_N, \quad (54)$$

$$\partial_z u(\mathbf{x}) = \check{T}^{-1}(i\underline{n}\hat{u}) \quad \forall \mathbf{x} \in X_N. \quad (55)$$



Here, with a slight abuse of notation, the left hand side is simply representing the respective expressions evaluated on the quadrature points in the real mesh  $X_N$ . Note that the nonlinear term is also generally in need of dealiasing, at least for the two periodic directions, but this is not discussed further in this paper.

#### 4. Implementation

An outline of the solution procedure, used for the numerical method described in Sec. 3, is given in Algorithm 1.<sup>1</sup> The major computational cost in Alg. 1 comes from computing the nonlinear convection and solving for Eqs. (44, 45). We consider in this section the linear solvers.

---

**Algorithm 1:** Solution procedure for Navier Stokes equations.

---

```

Initialize  $\mathbf{u}^0(\mathbf{x})$  and  $\mathbf{u}^1(\mathbf{x})$ 
Compute  $\hat{\mathbf{u}}_{\mathbf{k}}^0, \hat{\mathbf{u}}_{\mathbf{k}}^1, \hat{\mathbf{g}}_{\mathbf{k}}^0$  and  $\hat{\mathbf{g}}_{\mathbf{k}}^1$ 
Set parameters (e.g., mesh and viscosity) and end time  $T$ 
Compute LU decompositions of  $\check{H}(m, n), \bar{H}(m, n) \forall m, n \in K^p$ 
 $t \leftarrow \Delta t$ 
 $\kappa \leftarrow 1$ 
Compute nonlinear convection  $\hat{\mathcal{H}}_{\mathbf{k}}^0(\hat{\mathbf{u}}_{\mathbf{k}}^0, \hat{\mathbf{g}}_{\mathbf{k}}^0)$ 
while  $t < T$  do
    Compute nonlinear convection  $\hat{\mathcal{H}}_{\mathbf{k}}^{\kappa}$ 
    Compute right hand sides of Eqs. (44), (45)
    Solve Eq.(44) for  $\hat{\mathbf{u}}_{\mathbf{k}}^{\kappa+1} \forall \mathbf{k} \in \check{K}_N$ 
    Solve Eqs.(45) for  $\hat{\mathbf{g}}_{\mathbf{k}}^{\kappa+1} \forall \mathbf{k} \in \bar{K}_N$ 
    Solve Eqs.(46) for  $\hat{\mathbf{f}}_{\mathbf{k}}^{\kappa+1} \forall \mathbf{k} \in \bar{K}_N$ 
    Solve Eqs.(34, 35) for  $\hat{\mathbf{v}}_{\mathbf{k}}, \hat{\mathbf{w}}_{\mathbf{k}} \forall \mathbf{k} \in \bar{K}_N^0$ 
    Solve Eqs.(49, 50) for  $\hat{\mathbf{v}}^{\kappa+1}, \hat{\mathbf{w}}^{\kappa+1} \forall l \in \bar{K}^x, m = n = 0$ 
     $\kappa \leftarrow \kappa + 1$ 
     $t \leftarrow t + \Delta t$ 
    Update to new time step

```

---

Shen [13] writes that it is possible to solve Eq. (45) directly with essentially the same number of operations as a pentadiagonal solver. To this end, note that the matrix  $\bar{H}$  decouples into odd and even components, leading to two matrices of type upper Hessenberg. A direct LU decomposition (see, e.g., [21]), leads to a lower triangular matrix  $\bar{L}$  with only one subdiagonal and an upper triangular matrix  $\bar{U}$  that is dense. However, each row in  $\bar{U}$  contains at most three distinct values at  $\bar{U}_{k,k}, \bar{U}_{k,k+2}$  and  $\bar{U}_{k,k+4}$ , and then  $\bar{U}_{k,j} = \bar{U}_{k,k+4} \forall j = k + 6, k + 8, \dots, N_x - 2$ . Consequently only three diagonals in  $\bar{U}$  need storage and the back solve can be traversed very efficiently in  $\mathcal{O}(N_x)$ . Note also that the decoupling into odd and even coefficients leads to two subsystem that may be trivially solved simultaneously in two threads. For optimal performance, the odd and even coefficient would then

---

<sup>1</sup>Note that throughout this paper we are using the pseudocode conventions of Kopriva [20], with some minor differences. A vectorization statement like  $\{w_k\}_{k=0}^N \leftarrow \{u_k\}_{k=0}^N$  indicates that components  $u_k$ , for  $k = 0, 1, \dots, N$ , are copied from  $u_k$  to  $w_k$ . Similar conventions apply to matrices, e.g.,  $\{U_{1,k}\}_{k=0}^N = \{V_{2,k}\}_{k=0}^N$  can be used for copying row 2 of  $V$  to row 1 of  $U$ . Broadcasting is also implied, here meaning that for  $\{w\}_{k=0}^N \leftarrow c$ , where  $c$  is a scalar, all elements of  $w_k$  from  $k = 0$  to  $N$  gets the scalar value  $c$ .

need to be stored contiguously in computer memory, and not alternately, which would be the normal way of storing the coefficients.

The biharmonic problem in Eq. (44) is more challenging to solve for efficiently, but it is still possible, as suggested yet not devised by Shen [13], to find an algorithm that is  $\mathcal{O}(N_x)$  for a system of  $N_x$  unknowns. Note that  $\check{H}$  is the sum of three matrices  $\check{Q}$ ,  $\check{A}$  and  $\check{B}$ , and can be written as

$$\check{H} = \xi_0 \check{Q} + \xi_1 \check{A} + \xi_2 \check{B}, \quad (56)$$

where  $\xi_0, \xi_1$  and  $\xi_2$  are constants (depending on  $m$  and  $n$ ). The matrix  $\{\check{A}_{kj}\}_{k,j=0}^{N_x-4}$  contains only three nonzero diagonals at  $j = k - 2, k, k + 2$ , whereas matrix  $\{\check{B}_{kj}\}_{k,j=0}^{N_x-4}$  contains five nonzero diagonals at  $j = k - 4, k - 2, k, k + 2, k + 4$ . The nonzero elements of the upper triangular  $\{\check{Q}_{kj}\}_{k,j=0}^{N_x-4}$  matrix are given as [13]

$$\check{Q}_{kk} = -4(k+1)(k+2)^2, \quad (57)$$

$$\check{Q}_{kj} = p_k q_j + r_k s_j, \quad j = k+2, k+4, \dots, N_x-4, \quad (58)$$

where

$$p_k = 8k(k+1)(k+2)(k+4)\pi, \quad q_j = \frac{1}{j+3}, \quad (59)$$

$$r_k = 24(k+1)(k+2)\pi, \quad s_j = \frac{(j+2)^2}{(j+3)}. \quad (60)$$

A straight forward direct LU decomposition (without pivoting) of  $\check{H}$  can be performed as shown in Alg. 2, which leads to a lower triangular matrix  $\{\check{L}_{kj}\}_{k,j=0}^{N_x-4}$  with two nonzero diagonals at  $j = k - 2$  and  $k - 4$  plus a unity main diagonal. The upper triangular matrix  $\check{U}$  is dense and as such a show stopper for an efficient back solve. However, we note that  $\{\check{U}_{kj}\}_{k,j=0}^{N_x-4}$  contains three distinct diagonals at  $j = k, k + 2$  and  $k + 4$ , whereas the remaining part can be expressed as

$$\check{U}_{kj} = \xi_0(a_k q_j + b_k s_j), \quad j = k+6, k+8, \dots, N_x-4 \text{ and } k \leq N_x-10, \quad (61)$$

where  $\{a_k\}_{k=0}^{N_x-10}$  and  $\{b_k\}_{k=0}^{N_x-10}$  are two new vectors that can be computed recursively from  $\check{L}$ , as shown in Alg. 3. If  $a$  and  $b$  are pre-computed, the total storage requirement for the complete LU decomposition is less than  $7N_x$ , since there are two diagonals for  $\check{L}$ , three for  $\check{U}$  plus  $a$  and  $b$ . The solution of the complete system can be obtained very quickly with one simple forward elimination and a back solve, where the back solve is very fast ( $\mathcal{O}(N_x)$ ) because of (61), leading to a formula for the backwards substitution of  $\check{U}_{kj}\hat{u}_j = y_k$  like (valid for  $k \leq N_x - 10$ )

$$\hat{u}_k = \left( y_k - \check{U}_{k,k+2}\hat{u}_{k+2} - \check{U}_{k,k+4}\hat{u}_{k+4} - \xi_0 a_k \sum_{\substack{j=k+6 \\ k-j \text{ even}}}^{N_x-4} q_j \hat{u}_j - \xi_0 b_k \sum_{\substack{j=k+6 \\ k-j \text{ even}}}^{N_x-4} s_j \hat{u}_j \right) / \check{U}_{kk}, \quad (62)$$

that only requires one new addition to the row-sums for each back-traversed row, see Alg. (4).

## 5. Verification and validation

We have in previous sections described a Navier-Stokes solver for channel flows applicable to large-scale simulations. We have devised algorithms for fast direct sparse solvers, scalar products, and for the necessary fast transforms between physical and spectral space. The complete solver

---

**Algorithm 2:** LU decomposition of biharmonic operator  $\check{H}$ . Current algorithm is using dense storage of  $\check{U}_{kj}$ , but no more than the 3 items per row need to be stored ( $\check{U}_{kk}$ ,  $\check{U}_{kk+2}$  and  $\check{U}_{kk+4}$ ) after the row is no longer needed in the for-loop below (as the loop is traversed to row  $k$ ,  $\check{U}_{m,j}$  is no longer needed for  $m < k - 4$ ).

---

**Function** LUBiharmonic( $\{\check{H}_{kj}\}_{k,j=0}^N$ )

**output:**  $\{\check{L}_{kj}\}_{k,j=0}^N$ ,  $\{\check{U}_{kj}\}_{k,j=0}^N$

integer  $M_e \leftarrow \lfloor N/2 \rfloor$

integer  $M_o \leftarrow \lfloor (N-1)/2 \rfloor$

$\{\hat{U}_{0,2j}\}_{j=0}^{M_e} \leftarrow \{\hat{H}_{0,2j}\}_{j=0}^{M_e}$

$\{\hat{U}_{1,2j+1}\}_{j=0}^{M_o} \leftarrow \{\hat{H}_{1,2j+1}\}_{j=0}^{M_o}$

$\check{L}_{20} \leftarrow \check{H}_{20}/\check{U}_{00}$

$\check{L}_{31} \leftarrow \check{H}_{31}/\check{U}_{11}$

$\{\hat{U}_{2,2j}\}_{j=1}^{M_e} \leftarrow \{\check{H}_{2,2j}\}_{j=1}^{M_e} - \check{L}_{20}\{\check{U}_{0,2j}\}_{j=1}^{M_e}$

$\{\hat{U}_{3,2j+1}\}_{j=1}^{M_o} \leftarrow \{\check{H}_{3,2j+1}\}_{j=1}^{M_o} - \check{L}_{31}\{\check{U}_{1,2j+1}\}_{j=1}^{M_o}$

**for**  $k = 4$  **to**  $N$  **do**

    integer  $M \leftarrow \lfloor \frac{N-k}{2} \rfloor$

$\check{L}_{k,k-4} \leftarrow \check{H}_{k,k-4}/\check{U}_{k-4,k-4}$

$\{\check{U}_{k,k+2j}\}_{j=-1}^M \leftarrow \{\check{H}_{k,k+2j}\}_{j=-1}^M - \check{L}_{k,k-4}\{\check{U}_{k-4,k+2j}\}_{j=-1}^M$

$\check{L}_{k,k-2} \leftarrow \check{U}_{k,k-2}/\check{U}_{k-2,k-2}$

$\{\check{U}_{k,k+2j}\}_{j=-1}^M \leftarrow \{\check{U}_{k,k+2j}\}_{j=-1}^M - \check{L}_{k,k-2}\{\check{U}_{k-2,k+2j}\}_{j=-1}^M$

**return**  $\{\check{L}_{kj}\}_{k,j=0}^N$ ,  $\{\check{U}_{kj}\}_{k,j=0}^N$

---

**Algorithm 3:** Recursive formula to compute  $\{a_k\}_{k=0}^{N_x-10}$ ,  $\{b_k\}_{k=0}^{N_x-10}$  in Eq. (61). Note that the lower triangular matrix  $\{L_{kj}\}_{k,j=0}^{N_x-4}$  contains only two nonzero subdiagonals and the parameters  $p_k$  and  $r_k$  are given in Eqs. (59) and (60) respectively.

---

**Function** ReduceAB( $\{\check{L}_{kj}\}_{k,j=0}^{N_x-4}$ )

**output:**  $\{a_k\}_{k=0}^{N_x-10}$ ,  $\{b_k\}_{k=0}^{N_x-10}$

**for**  $k = 0$  **to**  $1$  **do**

$a_k \leftarrow p_k$

$b_k \leftarrow r_k$

$a_{k+2} \leftarrow p_{k+2} - \check{L}_{k+2,k} a_k$

$b_{k+2} \leftarrow r_{k+2} - \check{L}_{k+2,k} b_k$

**for**  $k = 4$  **to**  $N_x - 10$  **do**

$a_k \leftarrow p_k - \check{L}_{k,k-2} a_{k-2} - \check{L}_{k,k-4} a_{k-4}$

$b_k \leftarrow r_k - \check{L}_{k,k-2} b_{k-2} - \check{L}_{k,k-4} b_{k-4}$

**return**  $\{a_k\}_{k=0}^{N_x-10}$ ,  $\{b_k\}_{k=0}^{N_x-10}$

---

---

**Algorithm 4:** Solve biharmonic Eq. (44) with pre-computed  $\{\check{U}_{kj}\}_{k,j=0}^N$ ,  $\{\check{L}_{kj}\}_{k,j=0}^N$  matrices, as well as the  $\{a_k\}_{k=0}^{N-6}$  and  $\{b_k\}_{k=0}^{N-6}$  vectors. The parameters  $q_j$  and  $s_j$  are given in Eqs. (59) and (60) respectively. The vector  $\{f_k\}_{k=0}^N$  contains the right hand side and  $\{\hat{u}_k\}_{k=0}^N$  is the solution.

---

**Function** LUSolveBiharmonic( $\{f_k\}_{k=0}^N, \{\check{U}_{kj}\}_{k,j=0}^N, \{\check{L}_{kj}\}_{k,j=0}^N, \{a_k\}_{k=0}^{N-6}, \{b_k\}_{k=0}^{N-6}, \xi_0$ )

```

output:  $\{\hat{u}_k\}_{k=0}^N$ 
  // Solve  $\check{L}_{kj}y_j = f_k$  by forward elimination
  for  $k = 0$  to  $1$  do
     $y_k \leftarrow f_k$ 
     $y_{k+2} \leftarrow f_{k+2} - \check{L}_{k+2,k}y_k$ 
  for  $k = 4$  to  $N$  do
     $y_k \leftarrow f_k - \check{L}_{k,k-2}y_{k-2} - \check{L}_{k,k-4}y_{k-4}$ 
  // Solve  $\check{U}_{kj}\hat{u}_j = y_k$  with back substitution
  for  $k = N$  to  $N-1$  step  $-1$  do
     $\hat{u}_k \leftarrow y_k / \check{U}_{k,k}$ 
     $\hat{u}_{k-2} \leftarrow (y_{k-2} - \check{U}_{k-2,k}\hat{u}_k) / \check{U}_{k-2,k-2}$ 
   $q^o \leftarrow 0.0$ 
   $q^e \leftarrow 0.0$ 
   $s^o \leftarrow 0.0$ 
   $s^e \leftarrow 0.0$ 
  for  $k = N-4$  to  $0$  step  $-1$  do
     $\hat{u}_k \leftarrow y_k - \check{U}_{k,k+2}\hat{u}_{k+2} - \check{U}_{k,k+4}\hat{u}_{k+4}$ 
    if  $k < N-5$  then
       $j \leftarrow k+6$ 
      if  $k$  is odd then
         $q^o \leftarrow q^o + \hat{u}_j q_j$ 
         $s^o \leftarrow s^o + \hat{u}_j s_j$ 
         $\hat{u}_k \leftarrow \hat{u}_k - \xi_0 q^o a_k - \xi_0 s^o b_k$ 
      else
         $q^e \leftarrow q^e + \hat{u}_j q_j$ 
         $s^e \leftarrow s^e + \hat{u}_j s_j$ 
         $\hat{u}_k \leftarrow \hat{u}_k - \xi_0 q^e a_k - \xi_0 s^e b_k$ 
     $\hat{u}_k \leftarrow \hat{u}_k / \check{U}_{kk}$ 
  return  $\{\hat{u}_k\}_{k=0}^N$ 

```

---

Table 1: Roundoff error of the Biharmonic and Helmholtz linear algebra solvers. The first three rows show results for Alg. (4) and matrix  $\check{H}(\underline{z}, \Delta t, \nu)$ , whereas the last three rows show results for matrix  $\bar{H}(\underline{z}, \Delta t, \nu)$ . Parameters are chosen as  $\nu = 1/5200$  and  $\Delta t = 10^{-5}$  and the numbers shown are for an average of 100 runs.

	$N_x$						
$\underline{z}$	64	128	256	512	1024	2048	4096
0	3.27e-15	8.36e-15	2.10e-14	2.65e-14	2.88e-14	2.83e-14	3.29e-14
200	5.77e-14	8.50e-14	1.03e-13	1.08e-13	1.06e-13	1.06e-13	1.14e-13
1800	2.37e-13	1.65e-12	3.41e-12	3.33e-12	3.94e-12	3.79e-12	3.35e-12
5400	1.76e-13	1.84e-12	1.24e-11	1.57e-11	1.58e-11	1.55e-11	1.51e-11
0	3.26e-15	7.83e-15	1.89e-14	2.47e-14	2.16e-14	2.31e-14	1.94e-14
200	3.34e-15	8.63e-15	2.04e-14	2.54e-14	2.19e-14	2.01e-14	2.08e-14
1800	3.09e-15	8.23e-15	1.82e-14	2.27e-14	2.04e-14	2.18e-14	2.12e-14
5400	3.15e-15	7.77e-15	1.88e-14	2.25e-14	2.22e-14	2.10e-14	2.02e-14

has been implemented in the open source code spectralDNS [17]. For MPI we are using a slab decomposition, as described by Mortensen [22], but parallel scalability is not considered here since all algorithms described in previous sections are executed in serial. In this section we will simply verify the implementation, and validate the method for large-scale simulations. To this end we will first study some simple 1D problems.

Roundoff errors are often causing problems for spectral methods. The roundoff error of the linear solver described for the biharmonic problem in Sec. 4, and similarly for the Helmholtz problem, may be estimated by the following approach: Let  $\{u_i\}_{i=0}^{N_x-4}$  be a uniformly distributed random vector of double precision in the interval  $(0, 1)$ . Compute the matrix vector product  $f = \check{H}u$  and then solve  $\check{H}v = f$ , using Algorithms 2, 3 and 4, for  $\{v_i\}_{i=0}^{N_x-4}$ . The roundoff error of the solution algorithm may then be found as  $\max\{|u_i - v_i|\}_{i=0}^{N_x-4} / \max\{|u_i|\}_{i=0}^{N_x-4}$ . For this experiment we use double precision and assume that  $\Delta t = 10^{-5}$  and  $\nu = 1/5200$ , that are reasonable parameters for a turbulent channel flow simulation at  $Re_\tau = 5200$ . Four different wavenumbers  $\underline{z} = (0, 200, 1800, 5400)$  are also chosen as representative for such large-scale simulations. The 1800 case corresponds to the highest wavenumber used for the resolution of the largest known channel simulations, performed by Lee and Moser [6], where maximum  $\underline{z} = \sqrt{m_{max}^2 + n_{max}^2} = \sqrt{(10240/8)^2 + (7680/6)^2} \approx 1800$ . The mesh in the wall-normal direction is varied from 64 to 4096 points, which also covers almost three times higher resolution than used by Lee and Moser. Results shown in the first three rows of Table 1 indicate that roundoff errors are not very pronounced, even for problems as large as  $N_x = 4096$ . Further, the roundoff errors increase only slowly with increasing the wavenumbers. Corresponding results are also computed for the Helmholtz matrix (48) and results are shown in the last three rows of Table 1. For the Helmholtz matrix roundoff errors are seen to be insignificant. Note that Chebyshev-Gauss points are used for the computations in Table 1 and that Chebyshev-Gauss-Lobatto points give very similar (slightly better) results.

To show that the solvers are scaling with size, we investigate the execution time for solving  $\check{H}v = f$  and  $\bar{H}v = f$  on a complete wavenumber mesh of size  $(N_x, 64, 64)$ . We use a MacBook Pro laptop with the 2.8 GHz intel Core i7 processor. The average time for one single solve is shown in Table 2, where the numbers in parenthesis are used to indicate scaling (unity would be perfectly  $\mathcal{O}(N_x)$ ). The scaling is seen to be close to linear, and variations are most likely due to how well datastructures fit in the cache. The ability to solve large-scale problems is evident.

The Orr-Sommerfeld equation (see, e.g., [23]) is further used to establish that we are solving the right equations, and that the accuracy of the solver is second-order in time. The Orr-Sommerfeld eigenvalue problem is first solved for  $Re = 8000$ , using the biharmonic Shen basis (8). The leading

Table 2: Execution time (in seconds) for one solve of the Helmholtz (45) and Biharmonic (44) problems. The numbers in parenthesis are computed as  $t_n/t_{n-1}/2$ , where  $t_n$  is the current solvers timing in row  $n$ .

$N_x$	Biharmonic	Helmholtz
64	5.15e-07 (0.00)	4.01e-07 (0.00)
128	1.05e-06 (1.02)	8.03e-07 (1.00)
256	2.13e-06 (1.01)	1.65e-06 (1.03)
512	4.39e-06 (1.03)	3.39e-06 (1.03)
1024	8.67e-06 (0.99)	6.98e-06 (1.03)
2048	1.75e-05 (1.01)	1.39e-05 (0.99)
4096	3.96e-05 (1.13)	3.03e-05 (1.09)
8192	7.95e-05 (1.00)	6.27e-05 (1.03)

eigenvalue/eigenvector pair is then added as a perturbation to a laminar, parabolic, base flow, leading to an initial field

$$u(x, y, t) = -\epsilon \Re\{\iota \xi(x) \exp(\iota(y - \lambda t))\}, \quad (63)$$

$$v(x, y, t) = 1 - x^2 + \epsilon \Re\{\xi'(x) \exp(\iota(y - \lambda t))\}, \quad (64)$$

where  $\xi(x)$  is the eigenvector,  $\lambda = 0.2470750602 + \iota 2.664410371 \cdot 10^{-3}$  the eigenvalue and  $\epsilon \in \mathbb{R}^+$  is a small positive constant. Note that if  $\epsilon$  is chosen as too big, then the initial/boundary value problem will not agree well with the linearized Navier-Stokes equations used in deriving the Orr-Sommerfeld equations, due to second-order terms. Likewise, if  $\epsilon$  is chosen as too small, then roundoff errors will be too large, since the perturbation is added to a base flow with magnitude of order unity. It turns out that  $\epsilon = 10^{-7}$  is a good compromise, and that a mesh of size  $128 \times 8 \times 2$  is accurate enough to isolate temporal errors. Since the evolution of the perturbation is known analytically, the  $L^2$ -norm of the deviation from this exact linearized solution is used as a measure of the error. We also compute the error in the perturbation energy by

$$E(t) = \frac{\langle \tilde{\mathbf{u}}(\mathbf{x}, t), \tilde{\mathbf{u}}(\mathbf{x}, t) \rangle}{\langle \tilde{\mathbf{u}}(\mathbf{x}, 0), \tilde{\mathbf{u}}(\mathbf{x}, 0) \rangle} - \exp(2\Im\{\lambda\}t), \quad (65)$$

where  $\tilde{\mathbf{u}} = [u, v - (1 - x^2)]$  represents the perturbation vector. Table 3 shows the computed errors using a final time of  $t = 50$ , corresponding to 2 flow-throughs, and a varying  $\Delta t$ . We observe, as expected, second-order accuracy in the  $L^2$ -norm in time. The error in the accumulated perturbation energy is also found to be close to second order. Table 4 shows the computed error as a function of spatial discretization, where the time step is kept constant at  $\Delta t = 10^{-3}$  for 50 steps. The spectral decay of the error, with increasing  $N_x$ , is evident, and there is little difference between using either Chebyshev-Gauss (GC) or Chebyshev-Gauss-Lobatto (GL) points. Note that there is no difference at all between GC and GL for the results shown Table 3.

The final test for this fully spectral Navier-Stokes solver is the pressure driven turbulent channel flow. First, to measure scaling of the complete 3-dimensional solver, we use a rather small turbulent Reynolds number of  $Re_\tau = 590$  and a small computational box of size  $N_x \times 32 \times 32$ . Since the resolutions in  $y$  and  $z$  directions are kept constant, the complete Navier Stokes solver should ultimately scale like  $\mathcal{O}(N_x \log N_x)$ , since it is a combination of linear algebra routines  $\mathcal{O}(N_x)$ , fast transforms  $\mathcal{O}(N_x \log N_x)$  and several elementwise array operations  $\mathcal{O}(N_x)$ . We show in Table 5 some timings for one single time step, increasing only the wall-normal discretization. We see that the total time scales approximately as  $N_x \log N_x$  for large  $N_x$  and linearly for small  $N_x$ . This shift happens since at small  $N_x$  the transforms are fast and linear operations, like elementwise multiplications, are

Table 3: Error in the Orr-Sommerfeld perturbation at  $Re = 8000$ , for the most unstable eigenmode, as a function of time step. The mesh size is  $128 \times 8 \times 2$ . The  $L^2$ -norm  $\|\bar{\mathbf{u}}\| = \sqrt{\langle \bar{\mathbf{u}}, \bar{\mathbf{u}} \rangle}$ , where  $\bar{\mathbf{u}} = \mathbf{u} - \mathbf{u}_{\text{exact}}$ , and the energy error is computed as Eq. (65). The numbers in parenthesis are showing the order of the error, computed as  $\log(\tau_i/\tau_{i-1})/\log(\Delta t_i/\Delta t_{i-1})$ , where  $i$  is the row number of the table and  $\tau$  represents the values of  $\|\bar{\mathbf{u}}\|$  or  $E(t = 50)$ .

$\Delta t$	$\ \bar{\mathbf{u}}\ (t = 50)$	$\int_{t=0}^{t=50} E(t)dt$
1.0000e-01	2.9005e-09 (0.000)	1.2775e-02 (0.000)
6.6667e-02	1.2877e-09 (2.003)	5.3068e-03 (2.167)
5.0000e-02	7.2559e-10 (1.994)	2.8939e-03 (2.108)
4.0000e-02	4.6445e-10 (1.999)	1.8138e-03 (2.094)
3.3333e-02	3.2257e-10 (1.999)	1.2418e-03 (2.078)
2.8571e-02	2.3701e-10 (1.999)	9.0307e-04 (2.066)
2.5000e-02	1.8148e-10 (1.999)	6.8608e-04 (2.058)

Table 4: Error in the Orr-Sommerfeld perturbation at  $Re = 8000$ , for the most unstable eigenmode, as a function of  $N_x$ . The time step  $\Delta t = 10^{-3}$  and the end time is  $t = 0.05$ . The  $L^2$ -norm  $\|\bar{\mathbf{u}}\| = \sqrt{\langle \bar{\mathbf{u}}, \bar{\mathbf{u}} \rangle}$ , where  $\bar{\mathbf{u}} = \mathbf{u} - \mathbf{u}_{\text{exact}}$ , and the energy error is computed as Eq. (65). GC and GL refer to Chebyshev-Gauss and Chebyshev-Gauss-Lobatto points, respectively.

$N_x$	$\frac{1}{\epsilon}\ \bar{\mathbf{u}}\ (t = 0.05)$		$\int_{t=0}^{t=0.05} E(t)dt$	
	GC	GL	GC	GL
16	3.23081791e-01	4.76365364e-01	3.35105681e-02	3.10940983e-03
32	5.71635963e-03	6.77845098e-03	2.57328408e-04	5.02990613e-05
64	6.99681587e-08	8.22331688e-08	1.75070691e-09	8.04535105e-10
128	5.06389229e-08	4.81745061e-08	1.01924047e-09	1.53428292e-09
256	4.89447535e-08	4.83040873e-08	8.40445491e-10	3.77475917e-09

Table 5: Computing time for one time step using 32 wavenumbers in each periodic direction and  $N_x$  points in the wall-normal direction. The Assemble and Solve columns show the time required to assemble the right hand side (should be  $\mathcal{O}(N_x \log N_x)$  due to transforms) and solve the linear systems, respectively. The number in parenthesis shows the scaling, and unity would mean  $\mathcal{O}(N_x \log N_x)$  for Total and Assemble, whereas it would indicate  $\mathcal{O}(N_x)$  for Solve.

$N_x$	Total ( $\frac{t_k}{t_{k-1}} \frac{\log N_x - 1}{2 \log N_x}$ )	Assemble ( $\frac{t_k}{t_{k-1}} \frac{\log N_x - 1}{2 \log N_x}$ )	Solve ( $\frac{t_k}{t_{k-1}} \frac{1}{2}$ )
32	0.010 (0.00)	7.83e-03 (0.00)	1.07e-03 (0.00)
64	0.019 (0.86)	1.53e-02 (0.88)	1.98e-03 (0.92)
128	0.040 (0.96)	3.23e-02 (0.97)	3.81e-03 (0.96)
256	0.085 (0.98)	6.77e-02 (0.98)	7.58e-03 (1.00)
512	0.185 (1.04)	1.53e-01 (1.07)	1.58e-02 (1.04)
1024	0.384 (0.99)	3.18e-01 (0.99)	3.13e-02 (0.99)
2048	0.816 (1.02)	6.98e-01 (1.05)	6.45e-02 (1.03)
4096	1.736 (1.03)	1.44e+00 (0.99)	1.28e-01 (0.99)

more dominating. We also see that the time for assembly of the right hand side is approximately  $\mathcal{O}(N_x \log N_x)$ , whereas the time for solving the linear systems is very nearly linear. Note that for fast transforms we are using the FFTW library [24], with planner effort set to FFTW\_MEASURE. The results in Table 5 are computed with GC points and dealiasing is performed with the 2/3-rule [25].

For the ultimate test of a fully turbulent flow, we use the turbulent Reynolds number  $Re_\tau = 2000$ , which has been simulated previously by Hoyas and Jiménez [7], Lozano and Jiménez [9] and Lee and Moser [6]. Lozano and Jiménez showed that a small box of size  $2 \times 2\pi \times \pi$  in  $x, y$ , and  $z$  directions, respectively, could be simulated with  $633 \times 1024 \times 1024$  collocation points (compact finite differences in wall-normal direction, Fourier in periodic) in order to capture all relevant one-point statistics found in much larger boxes. We use the same small computational box, with resolution of  $512 \times 1024 \times 1024$ , and expect the superior resolution properties of spectral methods to work in our favor. Furthermore, the driving force  $\beta$  was dynamically adjusted in time to keep the flux through the channel constant. Simulations were run on the Shaheen II supercomputer at KAUST, using 512 cores. With a time step of  $2 \cdot 10^{-5}$ , the solver used approximately 1 second per time step. After reaching steady state, statistics were sampled for 100,000 time steps (enough to converge first order statistics), and the average velocity is shown in Figure 1 in a dashed line, alongside the results obtained by Hoyas and Jiménez [7] in a dotted line. The difference is hardly visible, showing that the fully spectral Shen-Fourier solver is reliable and robust for  $Re_\tau = 2000$ . Furthermore, the results presented in Tables 1, 2 and 5 indicate that the solver is more than likely to be reliable for even higher Reynolds numbers and larger scales.

## 6. Conclusions

In this paper a spectral-Galerkin Navier Stokes solver amenable to large-scale turbulent channel flows has been described. In the wall-normal direction, the solver utilizes base functions suggested by J. Shen [13], constructed from Chebyshev polynomials. The solver uses Fourier decompositions in both periodic directions, and, as such, it is fully spectral in all spatial directions. To validate the method for large-scale simulations at high Reynolds numbers, we have shown that the roundoff errors are small, even for simulations twice the size of the largest simulations known to date [6]. The computational cost of the solver is shown to scale with the expected  $\mathcal{O}(N_x \log N_x)$ , for a mesh of size  $N_x \times N_y \times N_z$  ( $N_y$  and  $N_z$  kept constant), due to fast transforms. Direct solvers have been devised for Helmholtz and biharmonic coefficient matrices, and these have been shown to scale close to  $\mathcal{O}(N_x)$ , with insignificant roundoff errors. Furthermore, all required scalar product matrices and



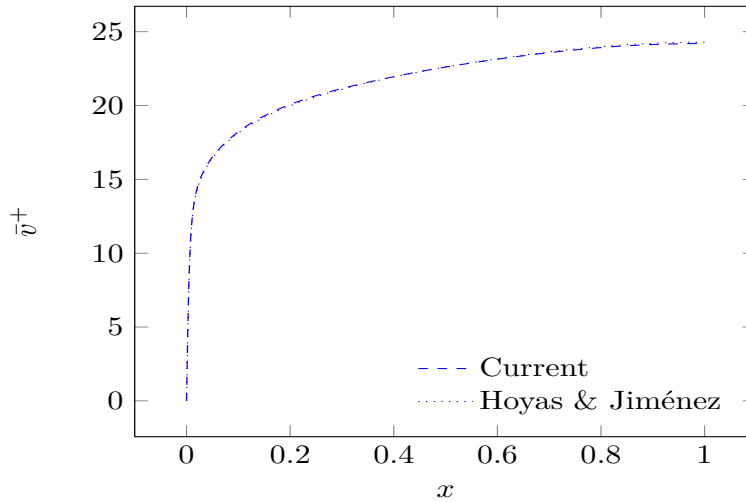


Figure 1: Average velocity  $\bar{v}^+ = \bar{v}/u_\tau$  in  $y$ -direction, for  $Re_\tau = 2000$ . Our results (dashed) are compared with those of Hoyas and Jiménez [7] (dotted).

fast transforms between spectral and physical space have been described. The fully spectral solver has been applied to a turbulent channel flow at  $Re_\tau = 2000$ , and the first order statistics are shown to agree well with the literature. The solver has been implemented as part of the open source project spectralDNS [17].

### Acknowledgements

This research is a part of the 4DSpace Strategic Research Initiative at the University of Oslo. I am also grateful to David Ketcheson and the KAUST Supercomputing Laboratory for providing access to Shaheen II.

### References

- [1] P. Moin, K. Mahesh, Direct numerical simulation: A tool in turbulence research, *Annual Review of Fluid Mechanics* 30 (1998) 539–578.
- [2] P. Moin, J. Kim, On the numerical solution of time-dependent viscous incompressible fluid flows involving solid boundaries, *Journal of Computational Physics* 35 (1980) 381 – 392.
- [3] L. Kleiser, U. Schumann, Treatment of Incompressibility and Boundary Conditions in 3-D Numerical Spectral Simulation of Plane Channel Flows, in: *3rd GAMM Conf. Numerical Methods in Fluid Mechanics*, 1980.
- [4] J. Kim, P. Moin, R. Moser, Turbulence statistics in fully developed channel flow at low Reynolds number, *Journal of Fluid Mechanics* 177 (1987) 133–166.
- [5] C. Canuto, M. Y. Hussaini, A. Quarteroni, T. A. Zang, *Spectral Methods in Fluid Dynamics*, Springer-Verlag New York-Heidelberg-Berlin, 1988. doi:10.1007/978-3-642-84108-8.

- [6] M. Lee, R. D. Moser, Direct numerical simulation of turbulent channel flow up to  $Re_\tau \approx 5200$ , *Journal of Fluid Mechanics* 774 (2015) 395–415.
- [7] S. Hoyas, J. Jiménez, Scaling of the velocity fluctuations in turbulent channels up to  $Re_\tau = 2003$ , *Physics of Fluids* 18 (2006).
- [8] S. Hoyas, J. Jiménez, Reynolds number effects on the Reynolds-stress budgets in turbulent channels, *Physics of Fluids* 20 (2008).
- [9] A. Lozano-Durán, J. Jiménez, Effect of the computational domain on direct simulations of turbulent channels up to  $Re_\tau = 4200$ , *Physics of Fluids* 26 (2014).
- [10] M. Bernardini, S. Pirozzoli, P. Orlandi, Velocity statistics in turbulent channel flow up to  $Re_\tau = 4000$ , *Journal of Fluid Mechanics* 742 (2014) 171–191.
- [11] S. K. Lele, Compact finite difference schemes with spectral-like resolution, *Journal of Computational Physics* 103 (1992) 16 – 42.
- [12] J. Shen, Efficient Spectral-Galerkin Method I. Direct Solvers of Second- and Fourth-Order Equations Using Legendre Polynomials, *SIAM Journal on Scientific Computing* 15 (1994) 1489–1505.
- [13] J. Shen, Efficient spectral-Galerkin method II. Direct solvers of second- and fourth-order equations using Chebyshev polynomials, *SIAM Journal on Scientific Computing* 16 (1995) 74–87.
- [14] F. Bouchon, F. Jauberteau, A multilevel method applied in the nonhomogeneous direction of the channel flow problem, *Applied Numerical Mathematics* 36 (2001) 1 – 34.
- [15] N. Hale, A. Townsend, A Fast, Simple, and Stable Chebyshev–Legendre Transform Using an Asymptotic Formula, *SIAM Journal on Scientific Computing* 36 (2014) A148–A167.
- [16] N. Hale, A. Townsend, A fast FFT-based discrete Legendre transform, *IMA Journal of Numerical Analysis* (2015).
- [17] spectralDNS, 2016. URL: <https://github.com/spectralDNS>.
- [18] Python, 2016. URL: [www.python.org](http://www.python.org).
- [19] Cython, 2016. URL: [www.cython.org](http://www.cython.org).
- [20] D. A. Kopriva, *Implementing Spectral Methods for Partial Differential Equations*, Springer Netherlands, 2009. doi:10.1007/978-90-481-2261-5.
- [21] G. W. Stewart, *Matrix Algorithms: Volume 1, Basic Decompositions*, SIAM, 1998.
- [22] M. Mortensen, H. P. Langtangen, High performance python for direct numerical simulations of turbulent flows, *Computer Physics Communications* 203 (2016) 53 – 65.
- [23] S. A. Orszag, Accurate solution of the Orr–Sommerfeld stability equation, *Journal of Fluid Mechanics* 50 (1971) 689–703.
- [24] M. Frigo, S. G. Johnson, The Design and Implementation of FFTW3, *Proceedings of the IEEE* 93 (2005) 216–231.
- [25] S. A. Orszag, On the Elimination of Aliasing in Finite Difference Schemes by Filtering High-Wavenumber Components, *Journal of the Atmospheric Sciences* 28 (1971) 1074.

## Appendix

*Fast scalar products and transforms.* Algorithms for fast scalar products and transforms, for the three spaces  $W_N, \bar{W}_N, \check{W}_N$ , see Eqs. (6, 7) and (8), are given in Alg. 5. The algorithms for the inverse transforms are given in Alg. 6. The algorithms are using the discrete cosine transforms (dct) of type 1, 2 or 3 depending on the choice of discretization points and direction.

*Matrices.* Matrices representing one-dimensional scalar products are given in Table 6. Note that the mass matrices are symmetrical, and as such only the upper triangular parts are described. Also note that the matrices are computed using quadrature, and not exact integration, which has some minor implications for Chebyshev-Gauss-Lobatto (GL) points. This follows since for an exact  $L_\sigma^2$  scalar product we would have  $c_{N_x} = 1$  for GL as well as Chebyshev-Gauss (GC), but for the  $l_\sigma^2$  scalar product used here  $c_{N_x} = 2$ . This disagreement, that follows from inexact quadrature at the highest mode, explains the inclusion of the  $c_{k+4}$  term for matrix  $\check{B}$ , and the  $c_{k+2}$  term for matrix  $\bar{B}$ . These are missing from Lemma 2.1 and 3.1 of [13], because Shen here considers only the exact  $L_\sigma^2$  scalar product.

---

**Algorithm 5:** Forward scalar products and transforms for all spaces  $W_N, \bar{W}_N, \check{W}_N$ . Here "dct" is the discrete cosine transform from SciPy. The matrices  $B, \bar{B}$  and  $\check{B}$  are given in Table 6.

---

```

Function forwardScalar( $\{f_j\}_{j=0}^N, points, space$ )
  output:  $\{y_k\}_{k=0}^N$ 
  if  $points = "Chebyshev-Gauss"$  then
     $\{w_k\}_{k=0}^N \leftarrow \text{dct}(\{f_j\}_{j=0}^N, \text{type}=2, \text{axis}=0) \frac{\pi}{2N}$ 
  else if  $points = "Chebyshev-Gauss-Lobatto"$  then
     $\{w_k\}_{k=0}^N \leftarrow \text{dct}(\{f_j\}_{j=0}^N, \text{type}=1, \text{axis}=0) \frac{\pi}{2(N-1)}$ 
     $\{y\}_{k=0}^N \leftarrow 0$ 
  if  $space = \bar{W}_N$  then
     $\{y_k\}_{k=0}^{N-2} \leftarrow \{w_k\}_{k=0}^{N-2} - \{w_k\}_{k=2}^N$ 
  else if  $space = \check{W}_N$  then
    for  $k = 0$  to  $N - 4$  do
       $y_k \leftarrow w_k - \frac{2(k+2)}{k+3}w_{k+2} + \frac{k+1}{k+3}w_{k+4}$ 
  else if  $space = W_N$  then
     $\{y_k\}_{k=0}^N \leftarrow \frac{2}{\pi}\{w_k\}_{k=0}^N$ 
     $y_0 \leftarrow y_0/2$ 
    if  $points = "Chebyshev-Gauss-Lobatto"$  then
       $y_N \leftarrow y_N/2$ 
  return  $\{y_k\}_{k=0}^N$ 

Function forwardTransform( $\{f_j\}_{j=0}^N, points, space$ )
  output:  $\{y_k\}_{k=0}^N$ 
   $\{y_k\}_{k=0}^N \leftarrow \text{forwardScalar}(\{f_j\}_{j=0}^N, points, space)$ 
  if  $space = \bar{W}_N$  then
     $\{y_k\}_{k=0}^{N-2} \leftarrow \{\bar{B}_{kj}^{-1}\}_{k,j=0}^{N-2} \{y_k\}_{k=0}^{N-2}$ 
  else if  $space = \check{W}_N$  then
     $\{y_k\}_{k=0}^{N-4} \leftarrow \{\check{B}_{kj}^{-1}\}_{k,j=0}^{N-4} \{y_k\}_{k=0}^{N-4}$ 
  else if  $space = W_N$  then
     $\{y_k\}_{k=0}^N \leftarrow \{B_{kj}^{-1}\}_{k,j=0}^N \{y_k\}_{k=0}^N$ 
  return  $\{y_k\}_{k=0}^N$ 

```

---

---

**Algorithm 6:** Inverse transforms for all spaces  $W_N, \bar{W}_N, \check{W}_N$ . Here "dct" is the discrete cosine transform from SciPy.

---

```

Function inverseChebTransform( $\{f\}_{k=0}^N, points$ )
  output:  $\{y_j\}_{j=0}^N$ 
  if  $points = "Chebyshev-Gauss"$  then
     $\{y_j\}_{j=0}^N \leftarrow \text{dct}(\{f\}_{k=0}^N, \text{type}=3, \text{axis}=0)$ 
     $\{y_j\}_{j=0}^N \leftarrow \frac{1}{2}\{y_j\}_{j=0}^N + \frac{1}{2}f_0$ 
  else if  $points = "Chebyshev-Gauss-Lobatto"$  then
     $\{y_j\}_{j=0}^N \leftarrow \text{dct}(\{f\}_{k=0}^N, \text{type}=1, \text{axis}=0)$ 
     $\{y_j\}_{j=0}^N \leftarrow \frac{1}{2}\{y_k\}_{k=0}^N + \frac{1}{2}f_0$ 
    for  $j = 0$  to  $N$  do
       $y_j \leftarrow y_j + \frac{(-1)^j}{2}f_N$ 
  return  $\{y_j\}_{j=0}^N$ 

Function inverseShenTransform( $\{f_k\}_{k=0}^N, points, space$ )
  output:  $\{y_j\}_{j=0}^N$ 
   $\{z_k\}_{k=0}^N \leftarrow 0$ 
  if  $space = \bar{W}_N$  then
     $\{z_k\}_{k=0}^{N-2} \leftarrow \{f_k\}_{k=0}^{N-2}$ 
     $\{z_k\}_{k=2}^N \leftarrow \{z_k\}_{k=2}^N - \{f_k\}_{k=0}^{N-2}$ 
  else if  $space = \check{W}_N$  then
     $\{z_k\}_{k=0}^{N-4} \leftarrow \{f_k\}_{k=0}^{N-4}$ 
    for  $k = 0$  to  $N - 4$  do
       $z_{k+2} \leftarrow z_{k+2} - \frac{2(k+2)}{k+3}f_k$ 
    for  $k = 0$  to  $N - 4$  do
       $z_{k+4} \leftarrow z_{k+4} + \frac{k+1}{k+3}f_k$ 
   $\{y_j\}_{j=0}^N \leftarrow \text{inverseChebTransform}(\{z_k\}_{k=0}^N, points)$ 
  return  $\{y_j\}_{j=0}^N$ 

```

---

Table 6: Matrix notation and description for one dimensional scalar products. Note that  $c_0 = 2$  and  $c_k = 1$  for  $0 < k < N_x$ . For Chebyshev-Gauss points  $c_{N_x} = 1$ , whereas  $c_{N_x} = 2$  for Chebyshev-Gauss-Lobatto points. Also note that only the upper diagonals are described for the symmetric matrices.

Notation	Scalar product	Description
$\{\check{C}_{kj}\}_{k,j=0}^{N_x-4, N_x-2}$	$(\bar{\phi}'_j, \check{\phi}_k)_\sigma$	$\begin{cases} -\pi(k+1), & j = k-1, \\ 2\pi(k+1), & j = k+1, \\ -\pi(k+1), & j = k+3, \\ 0, & \text{otherwise.} \end{cases}$
$\{\bar{C}_{kj}\}_{k,j=0}^{N_x-2, N_x-4}$	$(\check{\phi}'_j, \bar{\phi}_k)_\sigma$	$\begin{cases} \pi(k-2)(k+1)/k, & j = k-3, \\ -2\pi \frac{(k+1)^2}{k+2}, & j = k-1, \\ \pi(k+1), & j = k+1, \\ 0, & \text{otherwise.} \end{cases}$
$\{C_{kj}\}_{k,j=0}^{N_x, N_x-2}$	$(\bar{\phi}'_j, T_k)_\sigma$	$\begin{cases} -\pi(k+1), & j = k-1, \\ -2\pi, & j = k+1, k+3, \dots, N_x-2 \\ 0, & \text{otherwise.} \end{cases}$
$\{\check{M}_{kj}\}_{k,j=0}^{N_x-4, N_x-2}$	$(\bar{\phi}_j, \check{\phi}_k)_\sigma$	$\begin{cases} -\pi/2 & j = k-2, \\ \frac{\pi}{2} \left( c_k + 2 \frac{k+2}{k+3} \right) & j = k, \\ -\frac{\pi}{2} \left( 2 \frac{k+2}{k+3} + c_{j+2} \frac{k+1}{k+3} \right) & j = k+2 \\ \frac{\pi}{2} \frac{k+1}{k+3} & j = k+4, \\ 0, & \text{otherwise.} \end{cases}$
$\{\check{B}_{kj}\}_{k,j=0}^{N_x-4}$	$(\check{\phi}_j, \check{\phi}_k)_\sigma$	$\begin{cases} \frac{\pi}{2} \left( c_k + 4 \left( \frac{k+2}{k+3} \right)^2 + c_{k+4} \left( \frac{k+1}{k+3} \right)^2 \right), & j = k, \\ -\pi \left( \frac{k+2}{k+3} + \frac{(k+4)(k+1)}{(k+5)(k+3)} \right), & j = k+2, \\ \frac{\pi}{2} \frac{k+1}{k+3}, & j = k+4, \\ 0, & \text{otherwise.} \end{cases}$
$\{\bar{B}_{kj}\}_{k,j=0}^{N_x-2}$	$(\bar{\phi}_j, \bar{\phi}_k)_\sigma$	$\begin{cases} \frac{\pi}{2}(c_k + c_{k+2}) & j = k, \\ -\frac{\pi}{2} & j = k+2, \\ 0, & \text{otherwise.} \end{cases}$
$\{B_{kj}\}_{k,j=0}^{N_x}$	$(T_k, T_j)_\sigma$	$\frac{c_k \pi}{2} \delta_{kj}$ .